



Solar Irradiance Variability Monitor for the Galileo Solar Space Telescope Mission: Concept and Challenges

Franciele Carlesso^{1*}, Jenny Marcela Rodríguez Gómez^{2,3}, Adriany Rodrigues Barbosa¹, Luis Eduardo Antunes Vieira^{1,4} and Alisson Dal Lago¹

¹National Institute for Space Research (INPE), São José Dos Campos, Brazil, ²NASA Goddard Space Flight Center, Greenbelt, MD, United States, ³The Catholic University of America, Washington, D.C., United States, ⁴Department of Physics and Astronomy, George Mason University, University Drive, Fairfax, VA, United States

OPEN ACCESS

Edited by:

Mario J. P. F. G. Monteiro,
University of Porto, Portugal

Reviewed by:

Matthew DeLand,
Science Systems and Applications,
Inc., United States

Sanjay Gosain,
National Solar Observatory,
United States

*Correspondence:

Franciele Carlesso
fccarlesso@gmail.com

Specialty section:

This article was submitted to
Stellar and Solar Physics,
a section of the journal
Frontiers in Physics

Received: 04 February 2022

Accepted: 11 May 2022

Published: 24 June 2022

Citation:

Carlesso F, Rodríguez Gómez JM, Barbosa AR, Antunes Vieira LE and Dal Lago A (2022) Solar Irradiance Variability Monitor for the Galileo Solar Space Telescope Mission: Concept and Challenges. *Front. Phys.* 10:869738.
doi: 10.3389/fphy.2022.869738

Long and reliable total solar irradiance (TSI) time series is one of the essential parameters for understanding solar contributions to climate change. The minor fluctuations of TSI in long timescales could impact the energy balance. Despite the improvement of accurate measurements provided by the instruments, at the time, long-term TSI variability and its effects had not been established. The space-borne radiometer era provided observations in short timescales from minutes to years. Therefore, this study presents an overview of irradiance observations, highlighting the importance of following its variability in different time scales. In this context, the Galileo Solar Space Telescope that has been developed by the Institute for Space Research (INPE), Brazil, includes the Irradiance Monitor Module with a radiometer cavity like the classical design and a next-generation compact radiometer.

Keywords: total solar irradiance (TSI), electrical substitution radiometer, solar variability, solar luminosity, Galileo solar telescope-mission goals

1 INTRODUCTION

The Galileo Solar Space Telescope (GSST) is the first Brazilian solar mission that aims to perform high-resolution solar observations to study the evolution of the magnetic structure and its impact on the Geospace. The GSST mission has been studied in a concurrent engineering environment to analyze the mission architecture alternatives to reach its scientific goals. This pre-phase A feasibility analysis was conducted in 2017, providing a complete technical solution for the GSST program comprising LEO (low-earth orbit) and GEO (geostationary orbit).

The GSST has three main objectives:

- 1) Understand the evolution of the magnetic structures of the outer layer of the Sun
- 2) Understand the Sun's influence on Earth's Climate
- 3) Understand the Sun's influence on the Geospace.

The proposed payload package consists of high-resolution and full disk (wide field of view) telescopes with spectropolarimeters in visible and ultraviolet wavelengths, an absolute radiometer, a particle detector, and a magnetometer. The GSST instruments road map includes the development of ground prototypes, tests, and investigation of innovative solutions following a space phase with formal space system development.

Despite improved accurate measurements provided by the radiometers over the last 2 decades, long-term TSI variability and its effects have not been established completely. TSI variability

TABLE 1 | Summary of the missions to monitor TSI since 1978. Some flights are under operation (UO).

Time	Instrument/flight	Nominal orbit information	Ref
1978–1993	HF/NIMBUS-7	Sun-synchronous near-polar orbit	[103, 104]
1980–1989	ACRIM1/SMM	Circular Earth orbit, altitude 569–566 km, inclination 28.5°	[105, 106]
1984–2005	ERBE/ERBS	Non-sun-synchronous circular orbit, altitude 600 km, inclination 57°	[107]
1985–1989	ERBE/NOAA-9	Sun-synchronous, altitude 860 km, polar orbiting inclination = 99°	[108, 109]
1986–1987	ERBE/NOAA-10	Sun-synchronous, altitude 860 km, polar orbiting inclination = 99°	[109, 110]
1991–2001	ACRIM2/UARS	Non-sun-synchronous, altitude 585 km, 57° inclination	[111, 112]
1992–1993	SOVA2/EURECA	Low Earth orbit, altitude 525 km, inclination 28.5°	[78, 113]
1996–UO	VIRGO/SoHO	Halo orbit around the Sun/Earth Lagrangian Point (L1)	[114]
2000–2013	ACRIM3/ACRIMSat	Sun-synchronous, altitude 683–724 km, near-polar orbit inclination 98.13°	[115, 116]
2003–2020	TIM/SORCE	Non-sun-synchronous, altitude 645 km, inclination 40°	[73, 116]
2010–2014	PREMOS and SOVAP/PICARD	Sun-synchronous, altitude 735 km, inclination 98.28°	[8, 79]
2013–2019	TIM/TCTE	Near-circular orbit, altitude = 400–850 km, inclination 0°–98.8° ¹	[73]
2017–UO	CLARA/NorSat-1	Sun-synchronous, altitude 586 km, inclination 97.6°	[75]
2018–UO	TIM/TSIS-1	Near-circular orbit of the ISS, altitude of ~400 km, inclination = 51.6° ²	[73]

attributed to surface magnetic changes is the most well-established mechanism. Therefore, an absolute radiometer is essential to complement the information to the GSST spectropolarimeters and better understand the physical phenomenon behind the solar activity and irradiance variability.

One of the critical aspects of irradiance variability is its influence on Earth's atmosphere. Thus, the solar radiation arriving at the Earth's atmosphere is the primary energy source. This energy is called total solar irradiance (TSI) when all integrated emissions over the entire electromagnetic spectrum are measured per unit area at an astronomical unit [1, 2]. The continuous monitoring and knowledge of the absolute TSI measurements are crucial for the Earth's climate models. The space observations have expanded our view and understanding of the solar variability impact, specifically on the Earth's atmosphere and climate, and the magnitude of the natural forcing. The continuity of monitoring seeks to improve TSI reconstructions and forecasts.

Understanding the order of magnitude among many phenomena that affect TSI requires strict requirements on radiometers' accuracy, cadence, and stability. TSI monitoring has not been a simple task, and it represents a variety of observational challenges. This study reviews total solar irradiance through instrumentation, physical mechanisms behind this variability and future perspectives. In **Section 2**, we described the total solar irradiance observations. In **Section 3**, solar influence on TSI variability is described. We show the inhomogeneity of the TSI modeled values from different heliographic latitudes. In **Section 4**, we described the electrical substitution radiometers and the status of current developments. Finally, the scope of the first spacecraft concept for the GSST mission also included the challenges and contributions for the TSI measurements in **Section 5**.

2 TOTAL SOLAR IRRADIANCE OBSERVATIONS

The first known ground measurement of solar radiation based on water calorimetry was carried out during the 1830s by Pouillet

[3]. Angstrom was the first to use electrically calibrated detectors, and this principle is the base for modern radiometers [4]. However, only a continuous era of satellites would overcome the TSI limitations of ground monitoring and insufficient instrument precision. TSI has been observed from the radiometers onboard satellites since 1978. The individual early instrument's accuracy of about 0.2% was not enough to detect such changes in the 11-years solar cycle [5]. The accuracy improvement in the modern radiometers is mainly due to the precision aperture location, new materials development, data acquisition, and feedforward control system [6]. As seen in **Table 1**, longer-period observations depend on several near-Earth observation missions with different design instruments, satellite attitudes, and instrument degradation.

The TSI observed values were inconsistent over the years due to earlier TSI measurement accuracy and absolute calibration of the radiometers. Since TIM/SORCE, launched in 2003, it has been understood that observation radiometers might have an issue with the absolute scale. The value of TSI by TIM showed $1361 \pm 1 \text{ W/m}^2$ in the minimum solar period, representing values $\sim 4 \text{ W/m}^2$ lower than other instruments at the time (ACRIM3 and VIRGO). TSI Radiometer Facility (TRF), designed to ground compare TSI radiometers using a cryogenic radiometer, contributed to accuracy improvements [7]. PICARD/PREMOS (2010) [8], TCTE/TIM (2013), and TSIS-1/TIM (2017)³ instruments were ground calibrated or validated on TRF. In addition, the end-to-end instrument calibrations reduced record series discrepancies essential to establishing the accepted TSI value. TIM/SORCE and VIRGO/SOHO operated for longer; however, the individual observations of most instruments do not exceed more than a decade. Thus, overlapping the different design instruments is a crucial international effort to understand the potential uncertainty

¹<https://directory.eoportal.org/web/eoportal/satellite-missions/content/-/article/ors-3>.

²<https://directory.eoportal.org/web/eoportal/satellite-missions/content/-/article/iss-tsis>.

³<https://spot.colorado.edu/~koppg/TSI/>.

sources. Also, the flight correction introduces an additional uncertainty in the absolute values making a long-time TSI reconstruction extremely hard.

From space, the measurements showed variations of about 1.6 W/m^2 (0.12%) in phase with sunspot number [9]. However, so far, the life cycle of a single instrument cannot provide a complete understanding of the effects of the TSI variation on the Earth's climate and solar physics study. Therefore, these investigations rely on the composites by TSI value from multiple instruments. Furthermore, the difference in the absolute values of TSI between instruments decreased from the first instrument in 1978. Despite the advances in the most recent radiometers, constructing a composite is extremely hard, mainly due to the in-flight corrections and individual degradations. In 2005, estimating the sources of uncertainty in a joint effort, including in-orbit degradation of different instruments, the values indicated varied from 0 (ERBE) to 2930 (PMO6V) ppm year $^{-1}$. The declared degradation of the ACRIM3 primary sensor has been 900 ppm during the 13 1/2 years [10]. The TIM shows primary sensor degradation of 200 ppm in 10 years [11]. The stability differences of each instrument in the orbit play a critical role in maintaining SI traceability in a spatial environment. Tracking the effects of uncertainties due to in-flight degradation provides data stability by representing the changes in instrument lifetime. In an analysis, Kopp 2014 [11] estimated the stability of 61, 34, 27, and 10 ppm year $^{-1}$ for ACRIM3, PREMOS, VIRGO, and TIM, respectively.

At present, the four composites combine data from different instruments: ACRIM [12], IRMB [13], PMOD [14], and a recent composite by Dudok de Wit et al. [15]. The ACRIM and PMOD composites are well-known compilations, and both have different approaches for merging data. Zacharias (2014), in an independent review, highlighted the data gap between the operation of ACRIM-I/SMM and ACRIM-II/UARS as a critical issue when there was no instrument for TSI monitoring but only less accurate TSI values for Earth radiation budget (ERB) [16]. The possible ACRIM gap (from Jul./89 to Oct./91), Nimbus7/ERB, and ERBS/ERBE inaccuracies make it more difficult, being one of the leading causes of differences between PMOD and ACRIM composites [16]. The recent composite by Dudok de Wit et al. [15] computed data using a new approach using a multiscale maximum likelihood estimator to create a composite that closely agrees with the PMOD composite. Our goal here is not to highlight concepts about composites and various methods but to point out that there is no one definitive consensus on a single TSI series, and it can impact the TSI long-term reconstructions.

3 SOLAR INFLUENCE ON TSI VARIABILITY

3.1 Influence of Convective Features

The convection feature associated with heat transport occurs in different sizes and lifetimes. Granulation is considered a convective phenomenon. The scale motion of granulations is $\approx 1 \text{ Mm}$ with typical lifetimes from 5 to 10 min, and

supergranulation scales is $\approx 30 \text{ Mm}$ (which map to the chromospheric network) with an average lifetime of 25 h [17–19]. Quiet Sun fields are connected to the supergranulation patterns [20]. In the Quiet Sun, the network is a reticular pattern outline of supergranular cells, with a strong field of $\sim 1 \text{ kG}$, while the cell interior, with a weaker field of $\sim 1 \text{ hG}$, is called internetwork [20, 21]. The network patterns dominantly occupy the quiet Sun forming a magnetic network that drives mass and energy into the corona and heliosphere [22]. Even during the maximum solar cycle, most of the solar surface fits as quiet Sun, and its influence on TSI variability on decadal to millennial timescales is still a subject of debate [23, 24].

McIntosh et al. (2011) [22] found an essential connection between the supergranular scale parameter variation and irradiance. They associated the reduction over the expected TSI on previous solar minima to chromospheric network and possible weaker quiet Sun field. Different scenarios are observed in the TSI reconstruction, especially during the Maunder minimum from 1645 to 1715; when the near disappearance of sunspots and heliospheric activity was still present [25–27]. The different model assumption diverges on TSI from about $\sim 1 \text{ W m}^{-2}$ to $\sim 6 \text{ W m}^{-2}$ from Maunder to current [24, 28–30]. The significantly higher reconstructions values were obtained by Egorova et al. (2018) [24] and Shapiro et al. (2011) [28], which considered a different approach for the quiet Sun. According to some estimates, the TSI increase since the Maunder minimum is below 1 W m^{-2} [29, 30]. According to Foukal & Lean 1990 [31], the TSI secular variation approaching 0.5–1.0% over the past century, given the low precision instrumentation and insufficient understanding of solar radiative dynamics [32]. The results are not a consensus and try to solve its uncertainty to describe the solar minimum-to-minimum trend accurately; it is essential for understanding the relationship between solar activity and Earth's climate [32–34]. The different observed scenarios attributed to the quiet Sun are associated with the data used or not in the models [35]. The quiet Sun observations require instruments sensitive enough for magnetic field characterization from weak polarization signals [36]. New high-resolution instruments have been impacted in physical models and theoretical quiet Sun understanding. The observations of Hinode's spectropolarimeter revealed horizontal magnetic flux estimated by the Zeeman effect [37]. Studying the magnetic structure differences in quiet Sun in Polar regions and low latitudes is more challenging using data from the ecliptic plane [38].

3.2 Influence of Solar Features

The magnetic features on the solar surface and their dynamics are accepted to describe the TSI variability.

Figure 1 shows an overview of the surface features and TSI composite by Dudok de Wit et al. [15]. It allows observing different photospheric features such as quiet Sun regions (5–50 G), faculae regions (50–150 G), and active regions (500–4000 G) [39], pointing out the TSI during the period of maximum and minimum solar activity. Depending on the time scale, the TSI variability is attributed to oscillations, granulation, sunspot evolution, facular variability, the longitudinal asymmetry

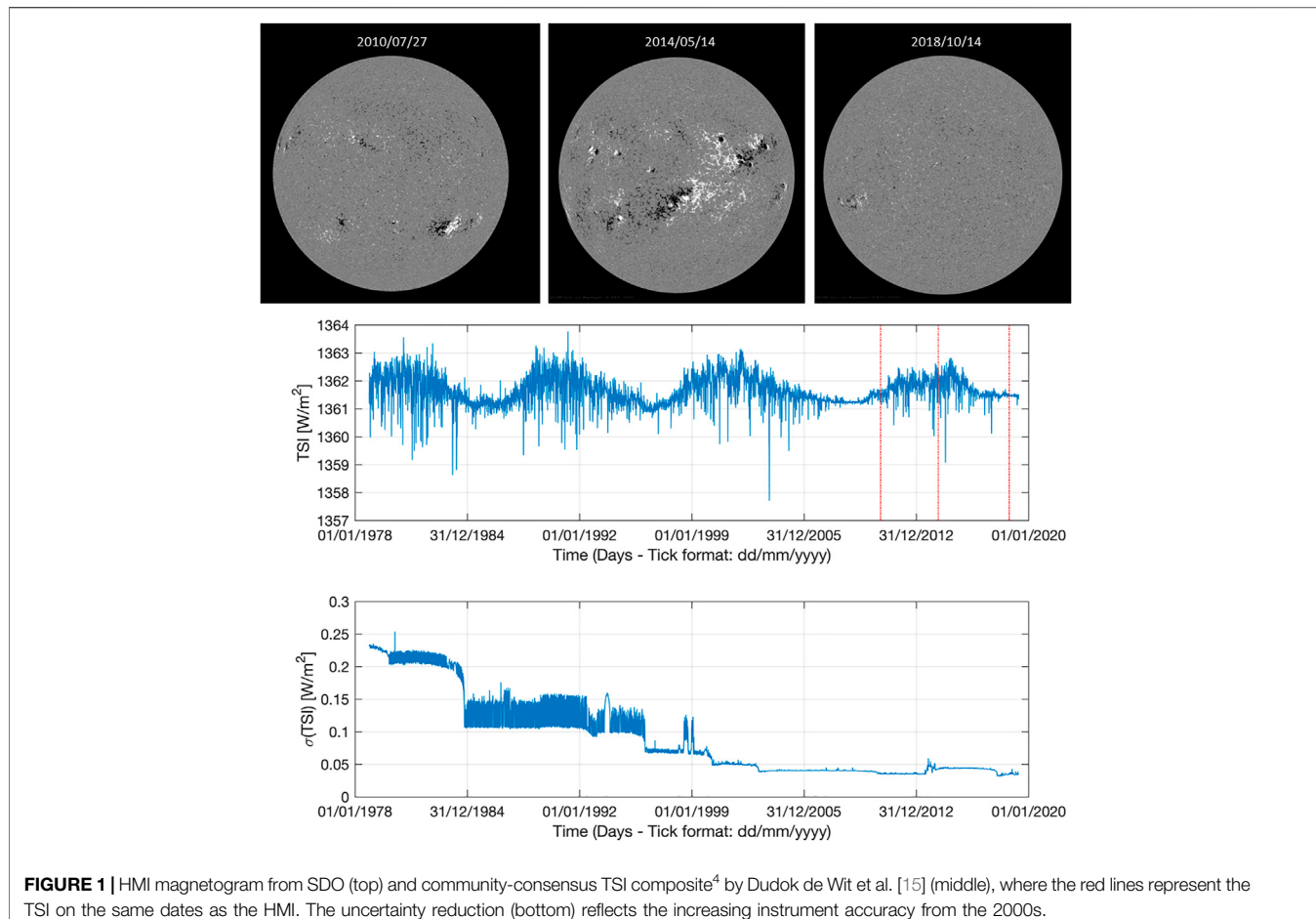


FIGURE 1 | HMI magnetogram from SDO (top) and community-consensus TSI composite⁴ by Dudok de Wit et al. [15] (middle), where the red lines represent the TSI on the same dates as the HMI. The uncertainty reduction (bottom) reflects the increasing instrument accuracy from the 2000s.

of the magnetic activity, and the active network [40]. The lifetime of a single instrument hardly reaches more than one complete solar cycle. It is not clear the mechanisms that affect TSI variability, especially for long periods (centuries or longer). Kopp (2014) [11] addresses the requirements to detect long-term variations such as entering or exiting the Maunder Minimum. The requirement instruments include the stability of continual measurements $< 0.001\%$ /year or sufficient absolute accuracy $< 0.01\%$ over a long period. The Solar irradiance variability models from days to years, i.e., solar cycles, are studied extensively during the last solar cycles. However, the variations in short timescales (of minutes or less) require additional studies.

Solar magnetism occurs at different timescales. Moreover, the various features are present in the entire hemisphere as active regions, sunspots, and magnetic pores or absence in times of low solar activity. Usually, the quiet Sun is denoted area outside sunspots, pores, and plages [20]. In addition, the solar surface subdivision based on the magnetic flux encompasses the quiet Sun, where the field is closed and weaker. While the active regions with sunspots, the magnetic field is the strongest and has mostly a closed field, and coronal hole regions include open magnetic field regions [17]. The combined influence of the convective motions, the

action of the magnetic field, the temperature stratification, and the differential rotation makes the analysis complex. For TSI variations from daily to the 11-years cycles, the primary mechanism is based on the evolution of the solar surface magnetic field, while on time scales of up to half a day, the granular convection becomes predominant [41].

TSI's cyclic changes are mainly attributed to the balance of excessive facular and magnetic network brightening and dark sunspots [58 and references therein]. The primary source of the daily or longer TSI variability is associated with the sunspots and faculae contribution [43]. The small sunspot lifetime can be as short as hours or days, while the large groups persist until months [44]. The link between the sunspot's motion across the Earth's visible side of the Sun and the decrease in TSI was first detected by the ACRIM I [45]. TSI can reduce as much as 0.34% for large sunspots near solar disk center, and it is responsible for the deep daily decreases in the TSI variation [40]. Faculae tend to persist longer and are more distributed over the solar disc than sunspots. Faculae and network contribution in TSI reconstruction from models based on magnetic activity present additional challenges due to small-scale feature observations, complex morphology,

⁴https://spot.colorado.edu/~kopp/Tsi/TSI_Composite-SIST.txt.

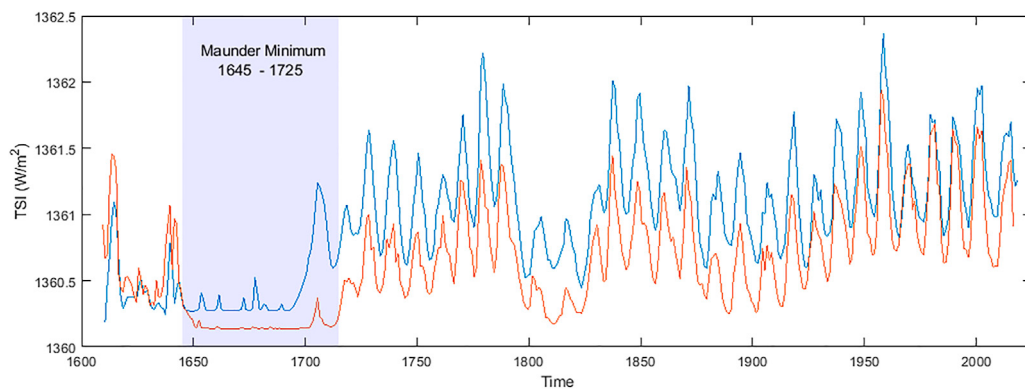


FIGURE 2 | Historical TSI reconstruction from 1610 to 2021. The comparison between Lean, J. L. [54]⁵ reconstruction (red line) and Koop, G reconstruction (blue line)⁶. The blue box highlights the Maunder minimum period from 1645 to 1715.

and weak contrast. While the relationship between the radiance and size is relatively well known for sunspots, the relationship between contrast and magnetogram signal for faculae and network is more complex [46, 47]. Interdecadal TSI variability manifests itself in amplitudes of consecutive 11-years cycles. Detecting the small-amplitude variations between the cycles is a scientific and technical challenge. The absolute value of total solar irradiance also shows a difference in the minimum levels, especially at the beginning of the series. The findings may indicate long-term changes [48]. The differences in the TSI level at solar minimums represent a limit to merging the TSI of different instruments in a single series and the long-term reconstructions [42, 49, 50].

Magnetic field indices and magnetic activity proxies usually are used in TSI models and predictions. There are several TSI variability models based on the solar surface features. The evaluation of irradiance increase usually employs chromospheric proxies, while the irradiance reduction usually employs a photometric sunspot index [51]. Lately, the solar activity indicators and their impacts have undergone revisions, such as the number of sunspots [44, 52]. Therefore, the influence of international Sunspot number record revision on the TSI models is also analyzed. Kopp et al. (2016) [53] carried out a study where two different TSI models employed the Clette et al. (2014) [52]’s Sunspot number. The authors realized that the average solar irradiance did not change significantly in both Satire-T e NRLTSI2 models during the Maunder Minimum period of low solar activity (1645–1715). However, it is possible to notice fluctuations of greater amplitude in TSI in the solar cycle between the years 1700–1874. They suggested that the cycles of this period may be like the Modern Maximum at the end of the twentieth century. After 1985, the effect of the new sunspot number is insignificant since the difference between the sunspot records is small. That the models depend less on the number of sunspots for this present period is also relevant.

Figure 2 shows two recent historical TSI reconstructions. Lean, J. L. [54]’s reconstruction employs the NRLTSI2 model that incorporates proxy indicators of the sunspot and facular sources. The model uses direct locations sunspots observations;

however, from 1610 to 1882, the model used Hoyt and Schatten 1998) [44] and SILSO sunspots. While Koop, G. reconstruction⁷ used the SATIRE S&T model for years before 1650, the SATIRE-T model from Wu et al. 2018 [55], including recent revisions to Sunspot number records (SILSO V.2), and datasets of spacecraft-instrument era TSI composite from Dudok de Wit et al. (2017) [15]. This plot shows two possible scenarios, including the differences during the minimum solar activity.

Photospheric magnetic activity is considered the primary source of the TSI variability at solar rotation time scales and the solar cycle [56]. Therefore, TSI variability has been interpreted as the result of the magnetic activity impact due to its influence on the local temperature structure and, consequently, the radiant properties of the solar atmosphere [57]. Yeo et al. [57, 58] highlighted the other proposed mechanisms to explain the relationship between the solar cycle modulation and solar irradiance, but additional evidence is necessary from observations. As an example, the oscillations are driven by the Coriolis force (r-modes oscillations) [59], thermal shadowing related to the toroidal magnetic field [60, 61], and magnetic modulation of convective energy flux [62].

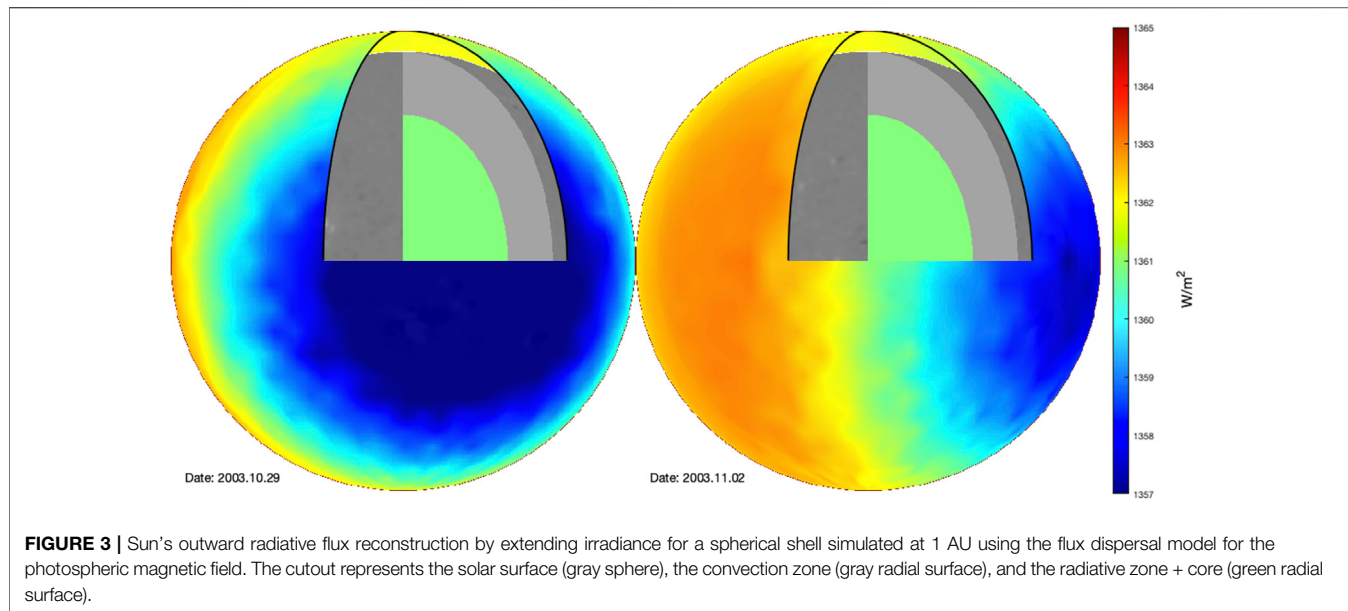
Short-term variability from minutes to hours is attributed to the globally-averaged superposition of solar convection and oscillations [40]. Additionally, the eruptive events as flares mainly observed in the UV and X-ray wavelengths occasionally affect the TSI variability. A short-duration increase in TSI of 0.028% was observed for some of the largest flares [40]. The precise contribution of the flares to TSI variation is unknown. However, it does not influence the radiative effect on the Earth’s climate [40].

The complex dynamics of the Sun influence the TSI variation at different temporal scales. The primary causes of change and its impact on the Earth are different for each time scale. Although the TSI variability on the Solar rotational time scale (~27 days) is not a direct climate direct forcing, spectral variations can affect the

⁵<https://agupubs.onlinelibrary.wiley.com/action/downloadSupplement?doi=10.1002%2F2017EA000357&file=ess2174-sup-0002-2017EA000357-ds01-.txt>.

⁶https://lasp.colorado.edu/lisird/data/historical_tsi/.

⁷<https://soppg.colorado.edu/~kopp/TSI/>.



Earth's upper atmosphere and consequently lead to climatic effects [40, 63]. The investigation of the physical mechanisms depends significantly on the device's cadence and high accuracy. The long-term measures have extra challenges due to degradation caused by exposure to the space environment and the need for in-orbit radiometer inter-calibration. Despite advances in radiometric measurements over the last decades, there are still many questions about variability and responsible physical mechanisms.

3.3 Orbital Variations and Their Influence on Solar Irradiance

Monitoring the solar flux density fluctuations is essential for the Earth-Sun coupled system study and providing knowledge of the Sun as a star. The TSI observations close to Earth from the ecliptic plane provide a near solar equatorial plane suitable for climatic studies. In comparison, the solar radiation observations from other points of view should explain TSI variability as a function of latitude. Furthermore, it estimates the Sun's luminosity and its temporal evolution. The TSI variability on the solar rotational time scale is associated with the passage of the bright and dark features in the solar disk. The depletion and increment on the TSI, integrated power per unit area at 1 AU, are affected by geometric factors depending on the relative position of the magnetic features on the solar surface and the observer.

Solar luminosity refers to the total electromagnetic power per unit of time output of the Sun; it is estimated empirically by extending the TSI model as the flux for the whole sphere. In comparison, the calculated TSI at 1 AU is estimated through the area and distribution of features on the disk [56, 64]. Vieira et al. (2012) [64] applied this approach to model the TSI as a function of the heliographic latitude indicating a non-equality of TSI levels at the hemispheres due to the imbalance of magnetic features. **Figure 3** illustrates the irradiance inhomogeneity on October 29, 2003, and November 03, 2003, when large sunspots were present on the solar disk. However, the current

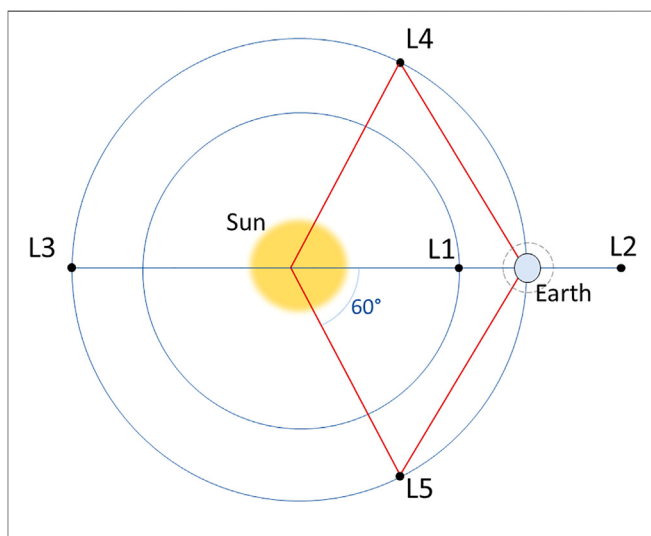


FIGURE 4 | Schematic of the Sun-Earth model with Lagrange point L1 to L5. All instruments have observed the TSI at near-Earth orbits save VIRGO/SOHO, which operates at L1.

impossibility of the far side and poles observation leads to a detailed knowledge lack of the local properties, limiting the improvement of reconstruction models [65]. Therefore, it is appropriate to complement the TSI measurements with an investigation of the magnetic structures for the physical interpretation of TSI variations. The instruments have carried out TSI observations at near-Earth orbits and Lagrangian Point (L1) (schematized in **Figure 4**). While missions such as the Solar Orbiter investigate the magnetic structures close up and out of the ecliptic plane (see **section 6**).

Expect L2; all Lagrange Points view the Sun continuously. The SOHO satellite operates around the L1 point. It has access to valuable and continuum information about the entire electromagnetic and particle spectrum of the Sun [66]. In a different approach to the Solar

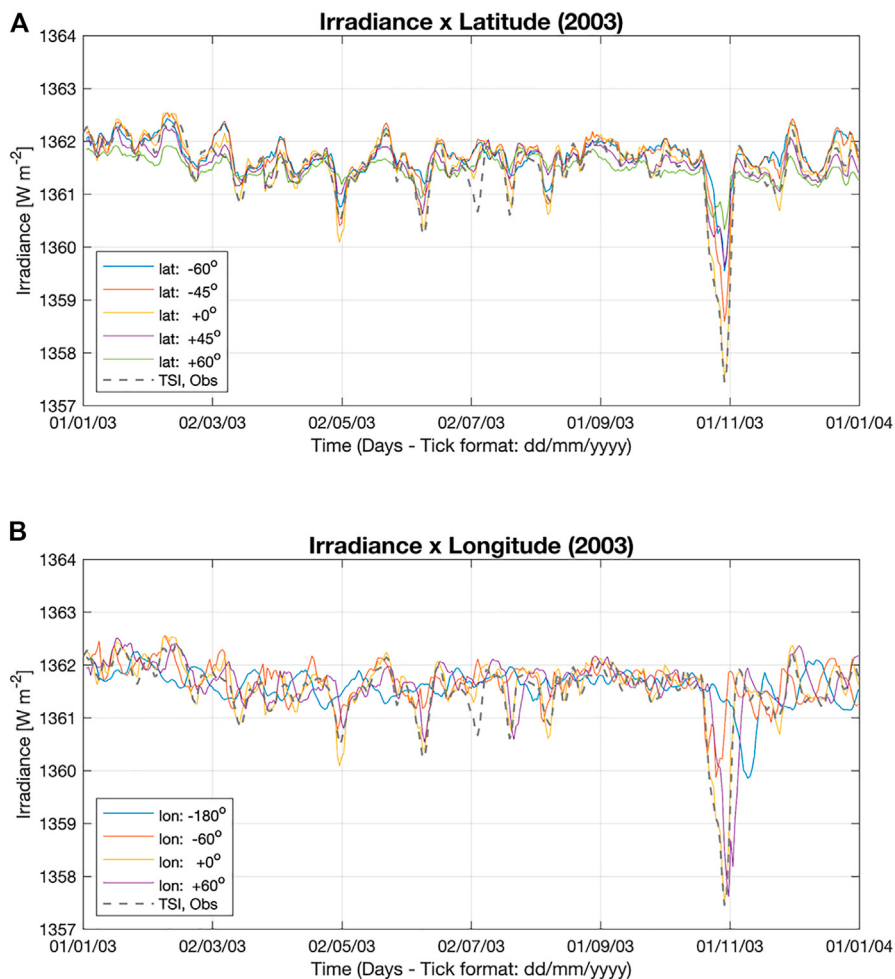


FIGURE 5 | Estimated TSI as a function of heliographic latitude **(A)** and longitude **(B)**.

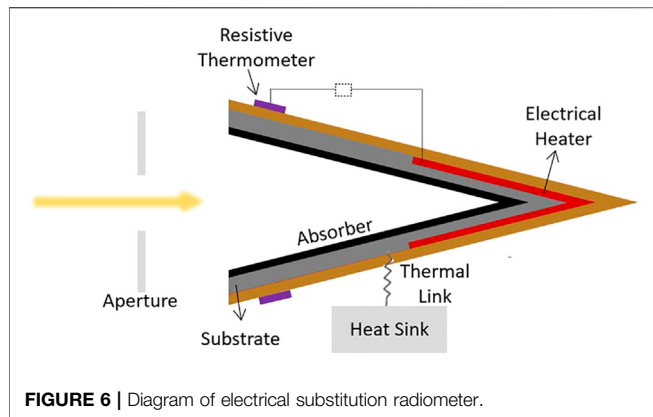
Orbiter, Parker Solar Probe spacecraft or “L1 L5 Together future Lagrange mission” [67], Bemporad (2021) [68] highlighted the advantages of future missions exploring L4 and L5 Lagrangian Points, instead of the convenience of the condition of L1 and L5 points by a twin mission to follow the evolution of magnetic fields. Notably, monitoring TSI from Lagrange points may provide the opportunity to expand our awareness of the Sun’s radiative output and, when combined with near-Earth observations, improve our understanding of its impact on Earth.

Figure 5 shows TSI as a function of the heliographic latitude and longitude regarding the point of view of the Lagrange Points. For TSI estimates, the distribution of the magnetic features made by the Helioseismic and Magnetic Imager (HMI) on the Solar Dynamics Observatory (SDO) [69] spacecraft was used. The TSI was estimated by extending a semi-empirical TSI model using the flux dispersal model for the photospheric magnetic field to reconstruct solar irradiance; this model was developed by Vieira et al. (2012) [64] and Vieira et al. (2022) [70]. The TSI observed only near the ecliptic plane is not able to represent the radiative outputs of the Sun. At higher latitudes, TSI does not follow the same decay compared to near the equator. Concerning

the inhomogeneity of irradiance in higher heliographic latitudes, the TSI decrease is less pronounced. Sunspots occur cyclically at latitude, typically around 40° in both hemispheres; as the cycle progresses, they move toward the equator [86]. The size and intensity of bright points are a heliographic function of angle [87], having a significant influence on TSI around 55° [80, 88]. Furthermore, a combined view of lon 0° , -60° , and 60° longitude will provide a central understanding of the influence of magnetic field evolution, especially the emergence and decay of the active regions, on the TSI. Our goal here is to point out that new viewpoint observations of TSI, such as from the Lagrange points, will improve the scientific knowledge about the influence of active regions and the quiet Sun on TSI.

4 ELECTRICAL SUBSTITUTION RADIOMETER FOR TSI MEASUREMENTS

This section analyses the radiometer design evolution to achieve enhanced performance in a space environment. Currently, the



instrument advances are closer to achieving the precision and stability requirements for the climate forcing models. On the other hand, for example, only the influence of large flares is detected even with low noise instruments. Short-term solar variability benefits from instruments with lower noise and higher cadences.

4.1 Background and Operating Principle

The thermal detectors are based on heating a body due to solar radiation absorption. Their operation compares electric Joule heating tracking some basic units. The radiometer's key components are a blackbody solar absorber, an electrical circuit for heating, a temperature-sensitive element, a thermal link, a heat sink, and a precision aperture to define incoming solar energy (Figure 6). The blackbody solar absorber usually performs in pairs. While the reference sensor is kept in the dark, the other sensor is exposed to solar radiation. The absorbed radiation will lead to a temperature gradient generating a heat flow through the heat sink. Once the system is in the vacuum environment, the voltage/current variations to keep the sensors thermally balanced equal the irradiance. The measured radiant flux (Φ) is written by Equation 1 regarding electrical heating (PE) and optical heating (PO) [71].

$$\Phi = K \cdot (P_E - P_O). \quad (1)$$

The correction factor (K) accounts for uncertainties if the electric and radiant heating does not fit perfectly. The slight differences in heat flow are part of the complex correction factor referred to as non-equivalence. The relation between electrical and optical power only has been guaranteed by the careful design of the critical components and each component's characterization and proper radiometer calibration. In order to measure the TSI, the characterization include analysis such as non-equivalence, cavity absorptance, radiation from background space, diffraction-losses, the Earth-Sun distance coefficient, Doppler-effect coefficient, for correction factor [72, 73].

In practice, the blackbody absorbers are cavities to improve the absorption of solar radiation. Commonly, the cavities are made of silver to increase thermal diffusivity along the cone [72–75]. ACRIM prevented heat transfer to the environment by aluminized Kapton shields [74], while TIM, CLARA, and

JTSIM plated gold outside to minimize the radiative losses. The typical geometries consist of a cone plus a cylinder [76], just the cylinder [77], cone, or inverted cone [78]. The measured reflectivity depends on the size and absorbing material. The cavities inside are coated with a black layer to absorb the solar radiation as diffuse black paint (MAP-PU1 [75], Nextel black velvet/3 M velvet [74, 79]), specular black paint (Z302 [80]), and etched Ni-P [73, 81]. For specular reflection coatings, the cone angle of ACRIM is 30°, and the PMO6 is 60° providing 5 or 6 internal reflections of an incident beam perfectly parallel to the optical axis [82]. However, a regular difficulty in paints or black Ni-P is to have a uniform coating on the tip of the cone resulting in beams of direct reflection on the bottom of the cone, reducing the cavity absorptivity. One solution found is the extension of a curved tube at the tip of the cone [83, 84].

The complex geometries are difficult to wire-wound heater around the cone or bonded some flexible circuit. Although the region heated electrically should be as close as possible to where the radiation hits, part of the scattered rays is absorbed in other parts of the cavity. The effects of non-equivalence are not the same for all detectors. In PMO6, due to inverted cone geometry, the first reflected radiation reaches the external cylinder, which is not electrically heated, producing an extra temperature gradient in that outer shield [82]. DIARAD and PMO6 estimated mismatches of electric and radiant heat consider the sensitivity mapping over the bottom of the cavity and along the sidewall with a laser beam [82]. In ACRIM, the non-equivalence below the 0.01% level was uncorrected at the time because of the assumptions about non-loss to outside [8]. Due to the phase-sensitive detection method, TIM estimated the non-equivalence uncertainty by characterizing the ratio between heater power and absorbed radiant power versus shutter frequency [73]. The effects of non-equivalence are minimized using high conductive material cavities, thin walls, a meticulous combination of electric and radiant heating, and ensuring the excellent connection of the interfaces, guaranteeing long periods of operation. In practice, the ultrasonic welding technique used in the DARA detector is an option implemented to connect cavity and heat link interfaces manufactured in one aluminum piece with the heat sink [72, 75].

The cavity reflectance value made at 633 nm for TIM and CLARA are in the order of 60 ppm [76] and 2000 ppm [75], but the length of the cavities is 6.34 cm [73] and 1.88 cm [75], respectively. The increase of the cavity size results in absorption enhancement. On the other hand, a larger cavity increases the time constant, determined by the thermal resistance and thermal capacity. Due to this limitation, the ESR's time constant will hardly be significantly reduced, especially for radiometers operating in a classical-complete cycle of measurement mode that could lead to excessive heating of the instrument [71]. Larger cavities in cryogenic radiometers work at approximately 4 K to decrease the specific heat [85]. Therefore, the instrument performance requires optimization of the thermal time constant and the sensitivity of the cavity. The detector is connected to a heat sink by a poor thermal link to ensure high sensitivity with a lower time constant and lower thermal mass. The contact and bonding between each part (cavity, resistor, heat link, and heat sink) affect the system's

thermal behavior. Additionally, the instruments use Joule heating in the current leads, and so careful thermal design for an appropriate correction is necessary to measure the uncertainty component of the heat dissipated through the receiver cavity before going to the heat sink and the rest of the heat that goes directly to the heat sink [86].

The cavity entrance is aligned with a precision aperture that defines the size of the solar beam, with diameters typically from 5 to 8 mm [73, 75, 82]. In traditional radiometers, sunlight is passed first through a view-limiting aperture and then through the precision aperture located close to the cavity. However, the discussions in the late 2000s led to the understanding that underestimating the internal scattering may have overestimated the solar irradiance. Since a fraction of the light is not captured by the baffles, it will occasionally reach the cavity. Therefore, PMO6 and DIARAD have a traditional design with a view-limiting aperture in front of the instrument to reduce stray light correcting the excess power of 1.001280 and 1.000833, respectively [86]. Otherwise, the TIM configuration, precision aperture in front of the instrument, and the field-of-the-view limiting aperture next to the cavity result in a power loss correction of 0.999582 [86]. The diffraction and scattering are associated with the aperture edge. These phenomenon components can be simulated, and their experimental distinction is a complex task to distinguish experimentally, both relevant in radiometry. The source-aperture-detector system is analyzed to understand the diffraction effect contribution. The assessment includes the extended source effect and wavelength proportionality [9, 21].

Furthermore, the precision aperture characterization requires analysis of material absorptivity, temperature effects such as a radiative component, and area variation due to expansion effects. The degradation processes of precision aperture materials are undeniable and may require extra care. Currently, the choice of the instrument includes aluminum [9], stainless steel, and tungsten carbide (85%) plus cobalt (15%) [8].

4.2 Degradation

The detector's degradation and aging in a space environment must be monitored for appropriate correction. The detector changes are tracked using a redundant cavity comparison from the ACRIM I [87] radiometer. Therefore, minimizing the exposure time of a cavity reduces the degradation allowing comparison with the frequently exposed cavity. TIM-mounted silicon photodiodes are used to monitor reflectivity changes of the cone [73]. Despite the instrument degradation monitoring for ACRIM series, VIRGO, and TIM, the degradation issues of in-flight instruments are still unresolved [23]. The directly exposed components are more sensitive to changes in mechanical and thermo-optical properties such as absorption and thermal emission. The environmental conditions depend on the instrument's operating orbit. The instrument degradation may be caused by an exposure to ultraviolet (UV) radiation, outgassing due to high vacuum levels, and atomic oxygen (AO) in low Earth Orbit (LEO). A key point is black coatings degradation; the paints usually have carbon as a pigment in a polymeric matrix that is more susceptible to damaging the organic chemical bonds or atomic oxygen erosion. On the other hand, the use of black Ni-P demonstrated greater robustness under space conditions [11].

4.3 Compact Designs

In recent years, some missions have made efforts to make the instrument compact to be suitable for Cubesats. Certainly, the instrument miniaturization requires both new designs and technological advances in critical aspects. The new materials with advanced properties can help us reshape the design of the new generation of radiometers. The main highlight is replacing the black Ni-P material with carbon nanotubes as an absorbent material in a silicon microfabrication sensor. Currently, RAVAN 3U CubeSat has demonstrated technologies for the Earth's radiation budget measurement and multipoint constellation. CSIM (Compact Spectral Irradiance Monitor), launched in 2018³, has been demonstrated as a suitable alternative for next-generation SSI monitoring technology. In line with this new generation of bolometers, a compact total irradiance monitor (CTIM) is under development for 6U CubeSat on silicon-based vertically aligned carbon nanotube (VACNT) [88]. VACNTs are currently known as the blackest material. In addition to the excellent absorption properties, VACNT has shown high performance by exposure to ionizing radiation doses typical of the LEO. The use of VACNT has also been evaluated for the interior of the conical-shaped cavity [89]. However, the fragility and high temperature required for VACNT growth by chemical vapor deposition (the most common method used for VANTA as black coatings) limits the use of some materials for other component incorporation. On CTIM, the commercial thermistors are bonded to the silicon and connected by conductive traces with wire bonds [88, 90]. The compact sensors represent advancement for bolometers showing the technological potential to achieve strict requirements. The innovative components and cost reductions have guided the goals of compact radiometers development.

5 IRRADIANCE MEASUREMENTS IN THE GSST MISSION

The internal institute stakeholders for the GSST mission include solar physics, solar-terrestrial physics, and climatology groups interested in TSI monitoring. Additionally, the Brazilian Space Study and Weather Monitoring Center (EMBRACE⁸, in Portuguese) uses an artificial network model [91] to compute the evolution of the TSI based on the irradiance variability due to the evolution of the solar magnetic field. **Table 2** summarizes the mission goals and objectives.

The TSI data will be utilized to understand the scientific objectives addressing the phenomena such as physical and dynamical solar properties, solar activity, and solar cycle. The GSST includes two instrument designs called irradiance monitor module (IMM) to achieve the mission goals. A cavity electrical substitution radiometer and a compact radiometer based on a photonic integrated circuit. The general IMM characteristics are outlined in **Table 3**. Both the radiometers will measure the TSI on the same platform. In addition, a classical cavity radiometer will

⁸<http://www2.inpe.br/climaespacial/portal/tsi-about/>.

TABLE 2 | Mission goals and objectives.

Goal 1: provide continuous high-accuracy and high-stability TSI measurement from space	
Objective 1.1	Absolute accuracy in the beginning of life of 0.03% (threshold), 0.01% (objective)
Objective 1.2	Stability of 0.001%/year
Objective 1.2	TSI measurements each 6 h means per day
Goal 2: Provide high-accuracy, high-stability, and high-cadence TSI measurement from space	
Objective 2.1	Absolute accuracy in the beginning of life of 0.01% (threshold), <0.01% (objective)
Objective 2.2	Stability of 0.001%/year
Objective 2.3	TSI measurement cadence of 60 s (threshold), 30 s (objective) during established observations

TABLE 3 | IMM main characteristics.

Parameter	Value
Mass	10 Kg
Power consumption	15 W
Spectral range	All
Design lifetime	5 years
Stability	0.001%/year
Nominal FOV	±2,5°

contribute to TSI monitoring over extended periods and intercalibration between the instruments.

As illustrated in **Figure 7**, the classical radiometer design takes advantage of advances described in **section 4**. The cavity is made of electroformed silver. It is coated internally with black Ni-P. This coating has a diffused reflectance of about 1% at 633 nm. The cavity design with a tube at the cone's apex makes it possible to produce a visually uniform black surface inside the cavity. The light reflected by the cavities is slightly more than 200 ppm. We employed ray-tracing software to study the region with the highest incidence of radiation. The heating resistance is formed by a wire wound outside the sensor positioned as close as possible to the place heated by the radiant power. The thermal links between the cavity and heat sink are stainless steel. A more detailed discussion of the approach to positioning the heating resistance on the sensor and heat flux between the cavity and the heat sink can be found in [84, 92].

Meanwhile, the thermo-optical sensor technology test allows for achieving significantly lower cadences. However, according to the theory, ESRs have some significant inherent limitations that still need to be overcome: 1) non-equivalence of the measured optical power and the electric Joule heat; 2) the relationship between the thermal time constant and the sensitivity of the sensor; 3) large thermal noises in the electrical heater and temperature sensor limiting the signal-to-noise ratio (SNR) [71]. The compact radiometer design is improved mainly by combining the alternatives for temperature measurement method, servo system replacement, and solar absorptance materials. The ESR, a thermal detector, requires high thermal control to achieve the accuracy requirements of the measurements. Usually, the servo system controls temperature differences between the heat sink and cavities. The servo loop also controls cavity temperature by switching between optical and

electrical heating. Mach-Zehnder interferometer (MZI) can measure the small phase shifts for high-resolution analysis [93]. A laser beam is coupled to the waveguide on the optical sensor. A Y-junction splits the beam equally, and after a distance, the beams are recombined. The output signal depends on the phase difference, which is a function of effective refractive indices. The radiation absorption in one MZI arm results in a variation in the index of refraction due to the temperature variation. Therefore, a phase difference occurs between the two propagating arms, which originate a destructive interference in the output signal. The PID acts by controlling the system to return to the constructive interference mode making it possible to calculate the absorbed radiant flux. The compact planar sensor employing an integrated Mach-Zehnder interferometer (MZI) is a feasible alternative to minimize or overcome classical sensor limitations.

The IMM in GSST program complements the magnetic structures observed by the spectropolarimeter. Among the mission concepts considered for the GSST, for the first satellite, the Brazilian PMM (multi-mission platform), schematically represented in **Figure 8**, has been investigated as an alternative for the first spacecraft to meet the orbital conditions established in the pre-phase A feasibility study. In the analysis, the Sun-synchronous orbit with RAAN positioned at 6:00 AM is the most suitable. The orbit inclination is 97.749°, and the altitude is 601.599 km above the equator. The design mission lifetime is at least 5 years.

6 DISCUSSION AND PERSPECTIVES ABOUT TOTAL SOLAR IRRADIANCE OBSERVATIONS

Indeed, the TSI observations and reconstructions variability provide essential information, including the Intergovernmental Panel on Climate Change (IPCC)⁹. Special attention has been given to distinguishing regional and global temperature impacts from natural and anthropogenic forcing. The effect of the TSI variability on the 11-years solar cycle on short-term regional and seasonal climate anomalies is measurable [94]. However, measuring the TSI variability impact on a time scale of

⁹https://www.ipcc.ch/site/assets/uploads/2018/02/WG1AR5_all_final.pdf.

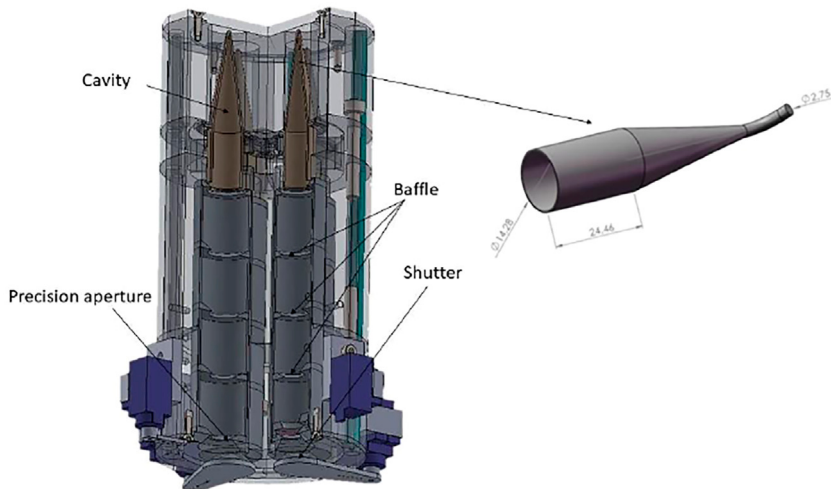


FIGURE 7 | Classical cavity radiometer schematic design.

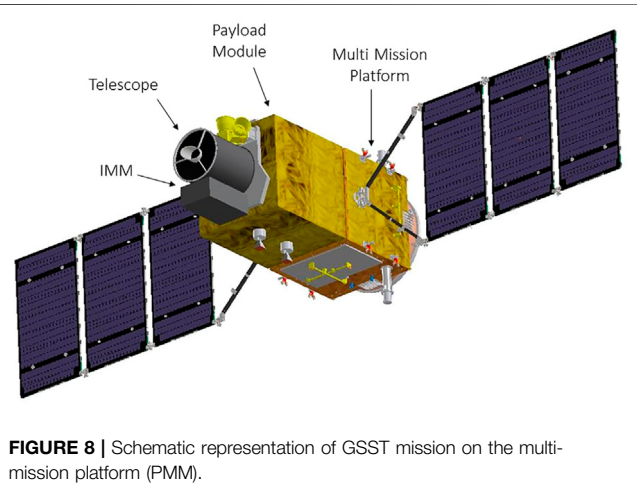


FIGURE 8 | Schematic representation of GSST mission on the multi-mission platform (PMM).

centuries or millennia introduces several additional challenges due to space degradation associated with difficulty in tracking SI-traceability.

Solar variability contributions to the past climate fluctuations or even predicting future influences require efforts. The main difficulties are the current series duration and the maintenance of uncertainty and stability of the instruments in space for long periods. A longer and more accurate TSI observation record should improve the understanding of the forcing variability effect. The solar irradiance models aim to explain the instrumental observations. While some models attribute TSI variability exclusively to the photospheric magnetic activity (sunspots, bright faculae, and bright network), others include phenomena such as the convective energy flux. The physical understanding and precise quantification require tracking information about magnetic features and TSI variability in accuracy and cadence compatible with the solar mechanisms.

The photospheric activity influences the total solar irradiance variations. However, this information about the magnetic activity comes from only the solar hemisphere facing the Earth. At the moment, the maps of non-visible disk or far side of the Sun are calculated using some techniques, i.e., seismic holography [95, 96], and the Global Oscillations Network Group (GONG) project has been producing daily far-side maps [97]. Ideally, the future new orbit missions should provide information about photospheric magnetic field and radiative output, extending the view of the Sun to the high-latitude and far side. Furthermore, the observations of the Sun out of the ecliptic plane allow us to determine the differences between poles and the solar equator; additionally, if the TSI variations observed near the Earth are attributed to luminosity variations or flux space contributions [98].

Determining the solar irradiance at all latitudes is one of the proposed science goals in the Voyage 2050 program [74]. In addition, to the solar poles investigation for extended periods, the POLARIS (POLAR Investigation of the Sun) mission intends to explore the development to achieve a satellite in a 0.48 AU circular orbit around the Sun with an inclination of 75° to the solar equator using a combination of a gravity assist and solar sail propulsion [75]. The Solar Orbiter (SO) mission, launched in 2020, combines *in situ* measurements in the Heliosphere or multiple telescope channels for remote imaging of the Sun and its atmosphere. This mission shows a unique short distance (minimum perihelion of 0.28 AU) and an orbit out of the ecliptic plane (18° and 30° helio-latitude during nominal and extended mission phase, respectively) [76]. Even without a TSI radiometer, the expected data from SO will contribute to the heliosphere investigation and the solar activity changes over time [99].

These missions present the critical challenges to the environment that affects the detectors, electronics, thermal effects of the platform, and payload, boosting new technological advances [100, 101]. Shortly, the results and new information about the solar dynamics and the latest technological advances will come from the SO. These can provide clues and knowledge to develop solar radiative energy flux

instrumentation or other detectors in extreme space conditions (inside solar corona).

Over the last decades, there has been significant improvement in the design and calibration of absolute radiometers but still requires improvements, including tracking degradation for appropriate in-flight correction. In addition, the observation instabilities can raise speculation about whether the inter-minima TSI decrease from 1996 to 2008 is authentic or instrumental and model limitation [76].

The radiometers' cross-calibrations and overlapping observations between the different instruments are essential to the TSI reconstruction. JTSIM includes two instruments, digital absolute radiometer (DARA) and the solar irradiance absolute radiometer (SIAR), on the same pointing system to monitor TSI at the same time in orbit for 8 years [72]. These observations can provide important information on each instrument's stability.

The GSST IMM module includes a classical cavity radiometer and a new miniaturized sensor. Its monitoring approach will provide information on solar irradiance variability in distinct timescales and magnitudes. The other key issue is to demonstrate new technologies to monitor TSI. The current radiometers follow the trend of miniaturization, seeking to maintain or improve performance. Compared to traditional cavity radiometers, compact technology has advantages in fabricating and characterizing flat sensors. Miniaturization is even more necessary to reduce overall mission costs and possible out-of-ecliptic orbit scenarios. They would be suitable for a new mission concept that seeks to develop technologies to fly closer to the Sun with small satellites as the effort of NIAC [102]. Especially, the GSST-designed sensor based on the photonic integrated circuit under development can be placed on a small satellite constellation for a better estimate of non-isotropic radiation reaching the Earth.

REFERENCES

1. Fedorov VM. Analysis of the Components of a Different Physical Nature in the Interannual Variability of the Total Solar Irradiance Flux. *Sol Syst Res* (2019) 53:376–82. doi:10.1134/S0038094619040026
2. Kopp G, Fehlmann A, Finsterle W, Harber D, Heuerman K, Willson R. Total Solar Irradiance Data Record Accuracy and Consistency Improvements. *Metrologia* (2012) 49:S29–S33. doi:10.1088/0026-1394/49/2/S29
3. Pouillet C-S-M. Mémoire sur la chaleur solaire: sur les pouvoirs rayonnants et absorbants de l'air atmosphérique et sur la température de l'espace (1838). Available at: <https://gallica.bnf.fr/ark:/12148/bpt6k95017r> (Accessed May 3, 2021).
4. Fröhlich C. History of Solar Radiometry and the World Radiometric Reference. *Metrologia* (1991) 28:111–5. doi:10.1088/0026-1394/28/3/001
5. Fröhlich C. Total Solar Irradiance Variations since 1978. *Adv Sp Res* (2002) 29:1409–16.
6. Kopp G. Solar Irradiance: Instrument-Based Advances. *Proc IAU* (2018) 14: 354–7. doi:10.1017/S1743921319004605
7. Kopp G, Heuerman K, Harber D, Drake G. The TSI Radiometer Facility: Absolute Calibrations for Total Solar Irradiance Instruments. *Proc SPIE* (2007) 6677:09. doi:10.1117/12.734553
8. Schmutz W, Fehlmann A, Finsterle W, Kopp G, Thuillier G. Total Solar Irradiance Measurements with PREMOS/PICARD. *AIP Conf Proc* (2013) 624–7. doi:10.1063/1.4804847
9. Kopp G, Lean JL. A New, Lower Value of Total Solar Irradiance: Evidence and Climate Significance. *Geophys Res Lett* (2011) 38:a–n. doi:10.1029/2010GL045777
10. Willson RC. ACRIM3 and the Total Solar Irradiance Database. *Astrophys Space Sci* (2014) 352:341–52. doi:10.1007/s10509-014-1961-4
11. Kopp G. An Assessment of the Solar Irradiance Record for Climate Studies. *J Space Weather Space Clim* (2014) 4:A14. doi:10.1051/swsc/2014012
12. Scafetta N, Willson RC. ACRIM Total Solar Irradiance Satellite Composite Validation versus TSI Proxy Models. *Astrophys Space Sci* (2014) 350:421–42. doi:10.1007/s10509-013-1775-9
13. Dewitte S, Crommelynck D, Mekaoui S, Joukoff A. Measurement and Uncertainty of the Long-Term Total Solar Irradiance Trend. *Sol Phys* (2004) 224:209–16. doi:10.1007/s11207-005-5698-7
14. Fröhlich C. Observations of Irradiance Variations. *Space Sci Rev* (2000) 94: 15–24. doi:10.1023/A:1026765712084
15. Dudok de Wit T, Kopp G, Fröhlich C, Schöll M. Methodology to Create a New Total Solar Irradiance Record: Making a Composite Out of Multiple Data Records. *Geophys Res Lett* (2017) 44:1196–203. doi:10.1002/2016GL071866
16. Zacharias P. An Independent Review of Existing Total Solar Irradiance Records. *Surv Geophys* (2014) 35:897–912. doi:10.1007/s10712-014-9294-y
17. Aschwanden MJ. *New Millennium Solar Physics*. Springer (2019). doi:10.1007/978-3-030-13956-8
18. Nordlund Å, Stein RF, Asplund M. Solar Surface Convection. *Living Rev Solar Phys* (2009) 6:6. doi:10.12942/lrsp-2009-2

DATA AVAILABILITY STATEMENT

The raw data supporting the conclusions of this article will be made available by the authors, without undue reservation.

AUTHOR CONTRIBUTIONS

Conceptualization: FC and LA. Software modeling: LA. Validation: LA. Formal analysis: FC and JR. Investigation: FC, JR, and AB. Resources: LA. Data curation: FC, JR, and AB. Writing—original draft preparation: FC. Writing—review and editing: JR and AD. Visualization: LA and AB. All authors have read and agreed to the published version of the manuscript.

FUNDING

This research was funded by grant 2021/13309–6, São Paulo Research Foundation (FAPESP), and grant 301991/2021-9 CNPq/PCI (*Programa de Capacitação Institucional*). AB thanks Capes (88887.607304/2021-00) and CNPq (141449/2021-7) for the financial support. LA thanks CNPq (Grant number 308355/2020-2) and the Brazilian Space Agency (Grant number TED AEB 2020–20VB—PO 0009).

ACKNOWLEDGMENTS

The authors would like to thank Adenilson Silva, Bráulio Fonseca Carneiro de Albuquerque, Ronan Arraes Jardim Chagas, and Graziela Maia for the technical support and analyses for the GSST platform.

19. Rieutord M, Rincon F. The Sun's Supergranulation. *Living Rev Solar Phys* (2010) 7. doi:10.12942/lrsp-2010-2
20. Bellot Rubio L, Orozco Suárez D. Quiet Sun Magnetic fields: an Observational View. *Living Rev Sol Phys* (2019) 16:1–124. doi:10.1007/s41116-018-0017-1
21. Chian AC-L, Silva SSA, Rempel EL, Gošić M, Bellot Rubio LR, Kusano K, et al. Supergranular Turbulence in the Quiet Sun: Lagrangian Coherent Structures. *Mon Not R Astron Soc* (2019) 488:3076–88. doi:10.1093/mnras/stz1909
22. McIntosh SW, Leamon RJ, Hock RA, Rast MP, Ulrich RK. Observing Evolution in the Supergranular Network Length Scale during Periods of Low Solar Activity. *ApJ* (2011) 730:L3. doi:10.1088/2041-8205/730/1/L3
23. Scafetta N, Willson RC. Comparison of Decadal Trends Among Total Solar Irradiance Composites of Satellite Observations. *Adv Astron* (2019) 2019:1–14. doi:10.1155/2019/1214896
24. Egorova T, Schmutz W, Rozanov E, Shapiro AI, Usoskin I, Beer J, et al. Revised Historical Solar Irradiance Forcing. *A&A* (2018) 615:A85–10. doi:10.1051/0004-6361/201731199
25. Beer J, Tobias S, Weiss N. An Active Sun throughout the Maunder Minimum. *Sol Phys* (1998) 181:237–49. doi:10.1023/A:1005026001784
26. Owens MJ, Usoskin I, Lockwood M. Heliospheric Modulation of Galactic Cosmic Rays during Grand Solar Minima: Past and Future Variations. *Geophys Res Lett* (2012) 39:a–n. doi:10.1029/2012GL053151
27. Usoskin IG, Arlt R, Asvestari E, Hawkins E, Käpylä M, Kovaltsov GA, et al. The Maunder Minimum (1645–1715) Was Indeed a Grand Minimum: A Reassessment of Multiple Datasets. *A&A* (2015) 581:A95. doi:10.1051/0004-6361/201526652
28. Shapiro AI, Schmutz W, Rozanov E, Schoell M, Haberreiter M, Shapiro AV, et al. A New Approach to the Long-Term Reconstruction of the Solar Irradiance Leads to Large Historical Solar Forcing. *A&A* (2011) 529: A67–8. doi:10.1051/0004-6361/201016173
29. Coddington O, Lean JL, Pilewskie P, Snow M, Lindholm D. A Solar Irradiance Climate Data Record. *Bull Am Meteorol Soc* (2016) 97:1265–82. doi:10.1175/BAMS-D-14-00265.1
30. Wang YM, Lean JL, Sheeley, Jr. NR, Jr. Modeling the Sun's Magnetic Field and Irradiance since 1713. *ApJ* (2005) 625:522–38. doi:10.1086/429689
31. Foukal P, Lean J. An Empirical Model of Total Solar Irradiance Variation between 1874 and 1988. *Science* (1990) 247(80-):556–8. doi:10.1126/science.247.4942.556
32. Scafetta N, Willson R, Lee J, Wu D. Modeling Quiet Solar Luminosity Variability from TSI Satellite Measurements and Proxy Models during 1980–2018. *Remote Sensing* (2019) 11:2569. doi:10.3390/rs11212569
33. Soon W, Connolly R, Connolly M. Re-evaluating the Role of Solar Variability on Northern Hemisphere Temperature Trends since the 19th century. *Earth Science Rev* (2015) 150:409–52. doi:10.1016/j.earscirev.2015.08.010
34. Scafetta N, West BJ. Estimated Solar Contribution to the Global Surface Warming Using the ACRIM TSI Satellite Composite. *Geophys Res Lett* (2005) 32:a–n. doi:10.1029/2005GL023849
35. Lockwood M, Ball WT. Placing Limits on Long-Term Variations in Quiet-Sun Irradiance and Their Contribution to Total Solar Irradiance and Solar Radiative Forcing of Climate. *Proc Math Phys Eng Sci* (2020) 476:20200077. doi:10.1098/rspa.2020.0077rspa20200077
36. Al-Janabi K, Al-Janabi K, Antolin P, Baker D, Bellot Rubio LR, Bradley L, et al. Achievements of Hinode in the First Eleven Years. *Publ Astron Soc Jpn* (2019) 71:1–118. doi:10.1093/pasj/psz084
37. Lites BW, Kubo M, Socas-Navarro H, Berger T, Frank Z, Shine R, et al. The Horizontal Magnetic Flux of the Quiet-Sun Internetwork as Observed with the Hinode Spectro-Polarimeter. *ApJ* (2008) 672:1237–53. doi:10.1086/522922
38. Prabhu A, Lagg A, Hirzberger J, Solanki SK. The Magnetic Fine Structure of the Sun's Polar Region as Revealed by Sunrise. *A&A* (2020) 644:A86–9. doi:10.1051/0004-6361/202038704
39. Gómez JMR, Carlesso F, Vieira LE, Da Silva L. A Irradiância Solar: Conceitos Básicos. *Rev Bras Ensino Fís* (2018) 40:40. doi:10.1590/1806-9126-rbef-2017-0342
40. Kopp G. Magnitudes and Timescales of Total Solar Irradiance Variability. *J Space Weather Space Clim* (2016) 6:A30. doi:10.1051/swsc/2016025
41. Seleznyov AD, Solanki SK, Krivova NA. Modelling Solar Irradiance Variability on Time Scales from Minutes to Months. *A&A* (2011) 532: A108–6. doi:10.1051/0004-6361/200811138
42. Mordvinov AV, Skakun AA, Volobuev DM. Long-term Changes in Total Solar Irradiance and Their Predictions. *Geomagn Aeron* (2018) 58:1175–86. doi:10.1134/S0016793218080248
43. Lean JL. Cycles and Trends in Solar Irradiance and Climate. *Wires Clim Change* (2010) 1:111–22. doi:10.1002/wcc.18
44. Dudok de Wit T, Lefevre L, Clette F. Uncertainties in the Sunspot Numbers: Estimation and Implications. *Sol Phys* (2016) 291:2709–31. doi:10.1007/s11207-016-0970-6
45. Willson RC. Solar Total Irradiance Variability Measurements by the SMM/ACRIM I Experiment. In: NASA, *Washington Solar Irradiance Variations on Active Region Time Scales* (2016). 1–42.
46. Yeo KL, Krivova NA. Intensity Contrast of Solar Network and Faculae. *A&A* (2019) 624:A135–18. doi:10.1051/0004-6361/201935123
47. Yeo KL, Solanki SK, Krivova NA. Intensity Contrast of Solar Network and Faculae. *A&A* (2013) 550:550A95. doi:10.1051/0004-6361/201220682
48. Fröhlich C. Evidence of a Long-Term Trend in Total Solar Irradiance. *A&A* (2009) 501:L27–L30. doi:10.1051/0004-6361/200912318
49. Domingo V, Ermoli I, Fox P, Fröhlich C, Haberreiter M, Krivova N, et al. Solar Surface Magnetism and Irradiance on Time Scales from Days to the 11-year Cycle. *Space Sci Rev* (2009) 145:337–80. doi:10.1007/s11214-009-9562-1
50. Dewitte S, Cornelis J, Meftah M. Centennial Total Solar Irradiance Variation. *Remote Sensing* (2022) 14:1072. doi:10.3390/rs14051072
51. Jain K, Hasan SS. Modulation in the Solar Irradiance Due to Surface Magnetism during Cycles 21, 22 and 23. *A&A* (2004) 425:301–7. doi:10.1051/0004-6361:20047102
52. Clette F, Svalgaard L, Vaquero JM, Cliver EW. Revisiting the Sunspot Number. *Space Sci Rev* (2014) 186:35–103. doi:10.1007/s11214-014-0074-2
53. Kopp G, Krivova N, Wu CJ, Lean J. The Impact of the Revised Sunspot Record on Solar Irradiance Reconstructions. *Sol Phys* (2016) 291:2951–65. doi:10.1007/s11207-016-0853-x
54. Lean JL. Estimating Solar Irradiance since 850 CE. *Earth Space Sci* (2018) 5: 133–49. doi:10.1002/2017EA000357
55. Wu C-J, Krivova NA, Solanki SK, Usoskin IG. Solar Total and Spectral Irradiance Reconstruction over the Last 9000 Years. *A&A* (2018) 620: A120–12. doi:10.1051/0004-6361/201832956
56. Krivova NA, Solanki SK, Fligge M, Unruh YC. Reconstruction of Solar Irradiance Variations in Cycle 23: Is Solar Surface Magnetism the Cause? *A&A* (2003) 399:399L1–L4. doi:10.1051/0004-6361:20030029
57. Yeo KL, Krivova NA, Solanki SK. Solar Cycle Variation in Solar Irradiance. *Space Sci Rev* (2014) 186:137–67. doi:10.1007/s11214-014-0061-7
58. Yeo KL. Analysis and Modeling of Solar Irradiance Variations. Dissertation. Braunschweig: Technischen Universität Carolo-Wilhelmina (2014).
59. Wolff CL, Hickey JR. Solar Irradiance Change and Special Longitudes Due to R-Modes. *Science* (1987) 80–235:1631–3. doi:10.1126/science.235.4796.1631
60. Kuhn JR, Libbrecht KG, Dicke RH. The Surface Temperature of the Sun and Changes in the Solar Constant. *Science* (1988) 80–242:908–11. doi:10.1126/science.242.4880.908
61. Kuhn JR, Bush RI, Scheick X, Scherrer P. The Sun's Shape and Brightness. *Nature* (1998) 392:155–7. doi:10.1038/32361
62. Cossette J-F, Charbonneau P, Smolarkiewicz PK. Cyclic thermal Signature in a Global MHD Simulation of Solar Convection. *ApJ* (2013) 777:L29. doi:10.1088/2041-8205/777/2/L29
63. Kopp G. Earth's Incoming Energy: The Total Solar Irradiance. In: S Liang, editor. *Comprehensive Remote Sensing*. Elsevier (2018). p. 32–66. doi:10.1016/B978-0-12-409548-9.10366-5
64. Vieira LEA, Norton A, Dudok De Wit T, Kretschmar M, Schmidt GA, Cheung MCM. How the Inclination of Earth's Orbit Affects Incoming Solar Irradiance. *Geophys Res Lett* (2012) 39:a–n. doi:10.1029/2012GL052950
65. Harral L, Andretta V, Appourchaux T, Baudin F, Bellot-Rubio L, Birch AC, et al. A Journey of Exploration to the Polar Regions of a star: Probing the Solar Poles and the Heliosphere from High Helio-Latitude. *Exp Astron* (2021). doi:10.1007/s10686-021-09769-x
66. Huber MCE, Bonnet RM, Dale DC, Arduin M, Fröhlich C, Domingo V, et al. The History of the SOHO Mission. *ESA Bull Nr* (1996) 86. Available at: <https://www.esa.int/esapub/bulletin/bullet86/huber86.htm> (Accessed September 5, 2021).
67. Hapgood M. L1L5Together: Report of Workshop on Future Missions to Monitor Space Weather on the Sun and in the Solar Wind Using Both the L1

- and L5 Lagrange Points as Valuable Viewpoints. *Space Weather* (2017) 15: 654–7. doi:10.1002/2017SW001652
68. Bemporad A. Possible Advantages of a Twin Spacecraft Heliospheric Mission at the Sun-Earth Lagrangian Points L4 and L5. *Front Astron Space Sci* (2021) 8:1–8. doi:10.3389/fspas.2021.627576
69. Schou J, Scherrer PH, Bush RI, Wachter R, Couvidat S, Rabello-Soares MC, et al. Design and Ground Calibration of the Helioseismic and Magnetic Imager (HMI) Instrument on the Solar Dynamics Observatory (SDO). *Sol Phys* (2012) 275:229–59. doi:10.1007/s11207-011-9842-2
70. Vieira LEA, Kopp G, Dudok De Wit T, da Silva LA, Carlesso F, Barbosa A, et al. Variability of the Sun's Luminosity Places Constraints on the thermal Equilibrium of the Convection Zone. *Astrophys J Suppl Ser* (2022). doi:10.48550/arXiv.2204.02940
71. Sapritsky V, Prokhorov A. Absolute Primary Radiometric Thermometry. In: *Blackbody Radiometry. Springer Series in Measurement Science and Technology*. Cham: Springer (2020). p. 545–664. doi:10.1007/978-3-030-57789-6_9
72. Song B, Ye X, Finsterle W, Gyo M, Gander M, Oliva AR, et al. The Fengyun-3E/Joint Total Solar Irradiance Absolute Radiometer: Instrument Design, Characterization, and Calibration. *Sol Phys* (2021) 296:296. doi:10.1007/s11207-021-01794-5
73. Kopp G, Lawrence G. The Total Irradiance Monitor (TIM): Instrument Design. *Sol Phys* (2005) 230:91–109. doi:10.1007/0-387-37625-9_610.1007/s11207-005-7446-4
74. Willson RC. Active Cavity Radiometer Type IV. *Sol Phys* (1980) 65:109. doi:10.1007/BF00151387
75. Walter B, Levesque P-L, Kopp G, Andersen B, Beck I, Finsterle W, et al. The CLARA/NORSAT-1 Solar Absolute Radiometer: Instrument Design, Characterization and Calibration. *Metrologia* (2017) 54:674–82. doi:10.1088/1681-7575/aa7a63
76. Heuerman K, Harber D, Ebbets A, Kopp G, Logan L. Calibration of the Absorptance Cavities for the Spaceflight Solar Radiometer TIM. *Proc Spieearth Observing Syst* (2006) XI. doi:10.1117/12.679668
77. Dewitte S, Crommelynck D, Joukoff A. Total Solar Irradiance Observations from DIARAD/VIRGO. *J Geophys Res* (2004) 109:1–8. doi:10.1029/2002JA009694
78. Romero J, Fröhlich C, Wehrli C. Solar Total Irradiance Variability Measured by SOVA-2 on Board EURECA. *Adv Space Res* (1995) 16:29–32. doi:10.1016/0273-1177(95)00263-E
79. Conscience C, Meftah M, Chevalier A, Dewitte S, Crommelynck D. The Space Instrument SOVAP of the PICARD mission. Proc Vol 8146. UV/Optical/IR Sp Telesc Instruments Innov Technol Concepts V. United States: San Diego, California (2011). p. 814613. doi:10.1117/12.895447
80. Kyle HL, Hoyt DV, Vallette BJ, Hickey JR, Maschhoff RH. Nimbus-7 Earth Radiation Budget Calibration History - Part I: The Solar Channels. *NASA Ref Publ* (1993) 1316.
81. Carlesso F, Vieira LEA, Berni LA, Savonov Gd. S, Remesal Oliva A, Finsterle W, et al. Physical and Optical Properties of Ultra-black Nickel-Phosphorus for a Total Solar Irradiance Measurement. *ApJS* (2020) 248:4. doi:10.3847/1538-4365/ab7af8
82. Fröhlich C. Solar Radiometry. In: MCE Huber, A Pauluhn, JL Culhane, JG Timothy, K Wilhelm, A Zehnder, editors. *Observing Photons in Space. ISSI Scientific Report Series*. New York, NY: Springer (2013). p. 565–81. doi:10.1007/978-1-4614-7804-1_32
83. Willson RC. Active Cavity Radiometer Type V. *Appl Opt* (1980) 19:3256–7. doi:10.1364/AO.19.003256
84. Carlesso F, Vieira LEA, Berni LA, Savonov Gd. S. Design, Implementation and Characterization of Cavity for Absolute Radiometer. *Front Phys* (2021) 9: 52. doi:10.3389/fphy.2021.598490
85. Fox N, Green P. Traceable Radiometry Underpinning Terrestrial- and Helio-Studies (TRUTHS): An Element of a Space-Based Climate and Calibration Observatory. *Remote Sensing* (2020) 12:2400. doi:10.3390/RS12152400
86. Butler JJ, Johnson BC, Rice JP, Shirley EL, Barnes RA. Sources of Differences in On-Orbital Total Solar Irradiance Measurements and Description of a Proposed Laboratory Intercomparison. *J Res Natl Inst Stand Technol* (2008) 113:187–203. doi:10.6028/jres.113.014
87. Willson RC, Gulkis S, Janssen M, Hudson HS, Chapman GA. Observations of Solar Irradiance Variability. *Science* (1981) 211:700–2. doi:10.1126/science.211.4483.700
88. Harber DM, Castleman Z, Drake G, Van Dreser S, Farber N, Heuerman K, et al. Compact Total Irradiance Monitor Flight Demonstration. In: *Proc. SPIE 11131, CubeSats and SmallSats for Remote Sensing III* (2019). doi:10.1117/12.2531308
89. Remesal Oliva A, Finsterle W, Walter B, Schmutz W. Characterisation of a New Carbon Nanotube Detector Coating for Solar Absolute Radiometers. *J Phys Conf Ser* (2018) 972:012007. doi:10.1088/1742-6596/972/1/012007
90. Tomlin NA, Yung CS, Castleman Z, Denoual M, Drake G, Farber N, et al. Overview of Microfabricated Bolometers with Vertically Aligned Carbon Nanotube Absorbers. *AIP Adv* (2020) 10:055010. doi:10.1063/5.0004025
91. Vieira LEA, Dudok de Wit T, Kretzschmar M. *Short-term Forecast of the Total and Spectral Solar Irradiance* (2011). arXiv e-printsarXiv:1111.5308.
92. Lopes AG, Irita RT, Berni LA, Vilela WA, da Silva Savonov G, Carlesso F, et al. Simplified Thermal Model for Absolute Radiometer Simulation. *J Sol Energ Eng* (2021) 143:1–6. doi:10.1115/1.4049939
93. Jackson DA, Dandridge A, Sheen SK. Measurement of Small Phase Shifts Using a Single-Mode Optical-Fiber Interferometer. *Opt Lett* (1980) 5:139. doi:10.1364/ol.5.000139
94. Bindoff NL, Stott PA, Achutarao KM, Allen MR, Gillett N, Gutzler D, et al. *Detection and Attribution of Climate Change: From Global to Regional* (2013). doi:10.1038/ncnoms13676
95. Braun DC, Lindsey C. Phase-sensitive Holography of Solar Activity. *Sol Phys* (2000) 192:307–19. doi:10.1007/978-94-011-4377-6_19
96. Braun DC, Lindsey C. Seismic Imaging of the Far Hemisphere of the Sun. *Astrophys J* (2001) 560:L189–L192. doi:10.1086/324323
97. Hernández IG, Jain K, Tobiska WK, Hill F. The Far-Side Solar Magnetic index. *J Phys Conf Ser* (2011) 271:012028. doi:10.1088/1742-6596/271/1/012028
98. Schmutz W, Fröhlich C, Rüedi I, Roth H, Wehrli C, Wyss J. SIM3D: Solar Irradiance Monitor-3d-View. In: *Solar Encounter. Proceedings of the First Solar Orbiter Workshop*. Spain: Puerto de la Cruz, Tenerife (2011). 447–50. Available at: <http://adsabs.harvard.edu/full/2001ESASP.493.447S>.
99. Müller D, Zouganelis I, St. Cyr OCOC, Gilbert HR, Nieves-Chinchilla T. Europe's Next mission to the Sun. *Nat Astron* (2020) 4:205. doi:10.1038/s41550-020-1015-5
100. Doherty KAJ, Carton JG, Norman A, McCaul T, Twomey B, Stanton KT. A thermal Control Surface for the Solar Orbiter. *Acta Astronautica* (2015) 117: 430–9. doi:10.1016/j.actaastro.2015.09.004
101. Doherty KAJ, Twomey B, McGlynn S, MacAuliffe N, Norman A, Bras B, et al. High-temperature Solar Reflector Coating for the Solar Orbiter. *J Spacecraft Rockets* (2016) 53:1077–84. doi:10.2514/1.A33561
102. Turyshev S, Helvajian H, Friedman LD, Heinsheimer T, Garber D, Davoyan A, et al. Exploring the Outer Solar System with Solar Sailing SmallSats on Fast-Transit Trajectories, In-Flight Autonomous Assembly of Advanced Science Payloads. *Bull AAS* (2021) 53:53. doi:10.3847/25c2cfb.b70177fe
103. Haas I, Shapiro R. The Nimbus Satellite System - Remote Sensing R&D Platform of the 70's. In: *American Institute of Aeronautics and Astronautics, 20th Aerospace Sciences Meeting*. Orlando) (1982). p. 14. doi:10.2514/6.1982-384
104. Kyle HL, Hoyt DV, Hickey JR. A Review of the Nimbus-7 ERB Solar Dataset. In: JM Pap, C Fröhlich, HS Hudson, WK Tobiska, editors. *The Sun as a Variable Star: Solar and Stellar Irradiance Variations*. Dordrecht: Springer (1994). p. 9–12. doi:10.1007/978-94-011-0950-5_2
105. Kramer HJ. Space Science/Solar-Terrestrial Missions. In: *Observation of the Earth and its Environment: Survey of Missions and Sensors*. Berlin, Heidelberg: Springer (2002). p. 863–982. doi:10.1007/978-3-642-56294-5_12
106. Willson RC, Hudson HS. Solar Maximum mission experiment: Initial Observations by the Active Cavity Radiometer. *Adv Space Res* (1981) 1: 285–8. doi:10.1016/0273-1177(81)90209-X
107. Barkstrom BR. The Earth Radiation Budget Experiment (ERBE). *Bull Amer Meteorol Soc*. (1984) 65 (11):11701185.
108. Barkstrom BR, Smith GL. The Earth Radiation Budget Experiment: Science and Implementation. *Rev Geophys* (1986) 24:379–90. doi:10.1029/RG024i002p00379
109. Matson M, Stephens G, Robinson J. Fire Detection Using Data from the Noaa-N Satellites. *Int J Remote Sensing* (1987) 8:961–70. doi:10.1080/01431168708954740

110. Barkstrom BR, Harrison EF, Lee RB. Earth Radiation Budget Experiment. *Eos Trans AGU* (1990) 71:297–304. doi:10.1029/EO071i009p00297
111. Reber CA, Trevathan CE, McNeal RJ, Luther MR. The Upper Atmosphere Research Satellite (UARS) mission. *J Geophys Res* (1993) 98:10643–7. doi:10.1029/92jd02828
112. Willson RC. UARS - ACRIM2 Observations and the Long Term Total Solar Irradiance Database. San Francisco, CA: AGU Fall Meeting (2001).
113. Nellessen W. The Development of the Roepan Trievable Rrier "EURECA". *Adv Space Res* (1995) 16:5–16. doi:10.1016/0273-1177(95)00260-L
114. Fröhlich C, Romero J, Roth H, Wehrli C, Andersen BN, Appourchaux T, et al. VIRGO: Experiment for Helioseismology and Solar Irradiance Monitoring. *Sol Phys* (1995) 162:101–28.
115. Willson RC, Helizon RS. EOS/ACRIM III Instrumentation. In: *Proc. SPIE 3750, Earth Observing Systems IV*. Denver (1999). doi:10.1117/12.363557
116. Parkinson CL, Ward A, King MD. *Earth Science Reference Handbook: A Guide to NASA's Earth Science Program and Earth Observing Satellite Missions* (2006). Available at: %5CBiblioteca_Digital_SPR%5CParkinson2006_NASA.pdf.

Conflict of Interest: The authors declare that the research was conducted in the absence of any commercial or financial relationships that could be construed as a potential conflict of interest.

Publisher's Note: All claims expressed in this article are solely those of the authors and do not necessarily represent those of their affiliated organizations, or those of the publisher, the editors, and the reviewers. Any product that may be evaluated in this article, or claim that may be made by its manufacturer, is not guaranteed or endorsed by the publisher.

Copyright © 2022 Carlesso, Rodríguez Gómez, Barbosa, Antunes Vieira and Dal Lago. This is an open-access article distributed under the terms of the Creative Commons Attribution License (CC BY). The use, distribution or reproduction in other forums is permitted, provided the original author(s) and the copyright owner(s) are credited and that the original publication in this journal is cited, in accordance with accepted academic practice. No use, distribution or reproduction is permitted which does not comply with these terms.